CHEMISTRY
A EUROPEAN JOURNAL

DOI: 10.1002/chem.200902494

Hydrogen Production by Water Dissociation in Surface-Modified $BaCo_xFe_yZr_{1-x-y}O_{3-\delta}$ Hollow-Fiber Membrane Reactor with Improved Oxygen Permeation

Heqing Jiang,*[a] Fangyi Liang,[a] Oliver Czuprat,[a] Konstantin Efimov,[a] Armin Feldhoff,[a] Steffen Schirrmeister,[b] Thomas Schiestel,[c] Haihui Wang,[d] and Jürgen Caro*[a]

Abstract: A porous perovskite $BaCo_xFe_yZr_{0.9-x-y}Pd_{0.1}O_{3-\delta}$ (BCFZ-Pd) coating was deposited onto the outer surface of a $BaCo_xFe_yZr_{1-x-y}O_{3-\delta}$ (BCFZ) perovskite hollow-fiber membrane. The surface morphology of the modified BCFZ fiber was characterized by scanning electron microscopy (SEM), indicating the formation of a BCFZ-Pd porous layer on the outer surface of a dense BCFZ hollow-fiber membrane. The oxygen permeation flux of the BCFZ membrane with a BCFZ-Pd porous layer increased 3.5 times more than that of the blank BCFZ membrane when feeding reactive CH_4 onto the permeation side of the membrane. The blank BCFZ membrane and surface-modified BCFZ membrane were used as reactors to shift the equilibrium of thermal water dissociation for hydrogen production because they allow the selective removal of the produced oxygen from the water dissociation system. It was found that the hydrogen production rate increased from 0.7 to 2.1 mL H_2 min^{-1} cm^{-2} at 950 °C after depositing a BCFZ-Pd porous layer onto the BCFZ membrane.

Keywords: heterogeneous catalysis · hollow-fiber membranes · oxygen separation · perovskite phases · water splitting

Introduction

Dense perovskite membranes with mixed oxygen ion and electron conductivity[1,2] have been intensively investigated as separator materials to produce pure oxygen from air[3] or in membrane reactors for the partial oxidation of methane (POM) to synthesis gas,[4] the oxidative dehydrogenation of light hydrocarbons (ODH) to olefins,[5] or in the Ostwald process.[6] It is accepted that oxygen permeation through a membrane involves 1) surface exchange between molecular oxygen and oxygen ions on the membrane surface and 2) bulk diffusion of the oxygen ion.[1] The diffusion-controlled oxygen permeation flux can be increased by reducing the thickness of the membrane until its thickness reaches a critical value. Below the critical thickness, the surface exchange processes become rate limiting. In this case, the oxygen permeation flux can be enhanced by coating the membrane with materials that show a high exchange rate, such as cobalt-containing perovskites[7] or noble-metal particles.[8] It is worth noting that the surface reaction accelerated by the active materials in the above work[7,8] is the oxygen ionization $O_2 + 4e^- \rightleftarrows 2O^{2-}$ because only the inert gas He was used to sweep the permeated oxygen.

[a] Dr. H. Jiang, F. Liang, O. Czuprat, K. Efimov, Dr. A. Feldhoff, Prof. J. Caro
Institute of Physical Chemistry and Electrochemistry
Leibniz University of Hannover, Callinstr. 3A
30167 Hannover (Germany)
Fax: (+49) 511-76219121
E-mail: heqing.jiang@pci.uni-hannover.de
juergen.caro@pci.uni-hannover.de

[b] Dr. S. Schirrmeister
Uhde GmbH, Friedrich-Uhde-Str. 15
44141 Dortmund (Germany)

[c] Dr. T. Schiestel
Fraunhofer Institute of Interfacial Engineering and Biotechnology (IGB)
Nobelstr 12, 70569 Stuttgart (Germany)

[d] Prof. H. Wang
School of Chemistry and Chemical Engineering
South China University of Technology
Guangzhou, 510640 (PR China)

Supporting information for this article is available on the WWW under http://dx.doi.org/10.1002/chem.200902494.

In another application of perovskite membrane as a reactor for the oxidation of light hydrocarbons,[1,5] the surface process is the reaction between the permeated oxygen species and the reactive gas, such as CH_4. In this case, a better reactor performance can be expected by coating the membrane with a catalytically active layer. However, to the best of our knowledge, no attention has been given, so far, to the surface modification of perovskite hollow-fiber membranes by a catalytically active porous layer. When the catalytic coating accelerates hydrocarbon oxidation, oxygen is consumed quickly, the driving force for oxygen permeation is increased, and a higher oxygen flux can be expected.

Recently, a novel $BaCo_xFe_yZr_{1-x-y}O_{3-\delta}$ (BCFZ) perovskite hollow-fiber membrane with high oxygen permeability has been developed in our group for oxygen separation or partial oxidation of methane to synthesis gas, for example.[9] Herein, we report on the surface modification of BCFZ hollow-fiber membrane by $BaCo_xFe_yZr_{0.9-x-y}Pd_{0.1}O_{3-\delta}$ (BCFZ-Pd) catalytic porous layer. The choice of BCFZ-Pd as the coating material is based on the following considerations: Compared with common catalysts such as Pd/Al_2O_3 that can lead to membrane failure due to the diffusion of Al and Co between the catalyst and membrane,[10] BCFZ-Pd shows a better compatibility with BCFZ membrane and has almost the same melting point as the perovskite BCFZ, which makes it possible to obtain a surface coating with good mechanical strength on the BCFZ membrane surface. Cobalt-containing perovskites and noble-metal Pd catalysts are known for their activity towards methane combustion.[11] The noble-metal, Pd-modified perovskites are expected to combine the advantages of the above two kinds of catalysts, namely, catalytic activity and thermal resistance. In addition, it was reported that the presence of Pd can increase the reducibility of cobalt ions in $Pd–Co/Al_2O_3$,[12] which leads to a better catalytic performance for methane oxidation. It can be expected, therefore, that the fine mixing of Pd and Co in the perovskite lattice will favor the interaction between them. The ionic radius of $Pd^{2+} = 80$ pm allows the modification of the B site of the $ABO_{3-\delta}$ structure according to the Goldschmidt tolerance concept. So a pure phase of Pd–Co-containing perovskite (BCFZ-Pd) was first prepared in this work.

Results and Discussion

Figure 1 presents the X-ray diffraction (XRD) pattern of BCFZ-Pd (4.2 wt% Pd) powder used in this work. From the absence of signals different from a pure perovskite phase, it is concluded that a one-phase material has been formed with Pd successfully incorporated into the BCFZ lattice. This can be further proven by transmission electron microscopy (TEM) results. Figure S1a and b (see the Supporting Information) show the dark-field micrograph of BCFZ-Pd particles and the energy-dispersive X-ray spectrum (EDXS) of the particles, respectively, which demonstrate the presence of Ba, Co, Fe, Zr, Pd, and O. The corresponding elemental distribution images (Figure S1c to h in the Supporting Information) show that all the elements were homogenously distributed in the particles. Electron diffraction pattern from a selected area of the BCFZ-Pd particle (Figure S2a and b in the Supporting Information) indicates that BCFZ-Pd has a singular crystal structure. Moreover, the crystal orientation can be observed from the high-resolution transmission electron microscopy (HRTEM) micrograph (Figure S2c in the Supporting Information). The results of XRD and TEM demonstrated the formation of a pure perovskite phase BCFZ-Pd and the homogeneous distribution of Co and Pd in the perovskite lattice.

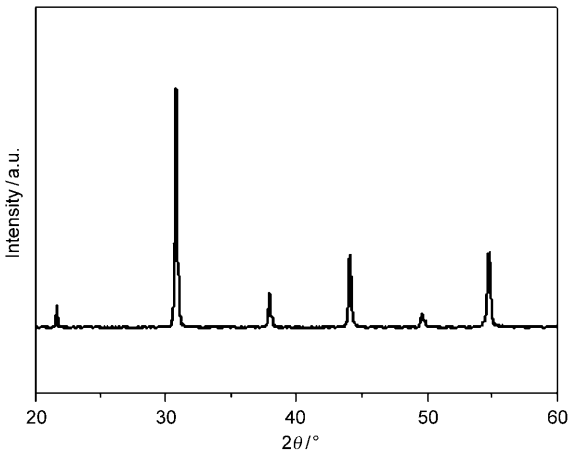

Figure 1. XRD pattern of the BCFZ-Pd powder used for coating the BCFZ hollow-fiber membranes.

It was experimentally found that the mechanical strength and porosity of the BCFZ-Pd coating layer on the surface of the BCFZ fiber can be adjusted by controlling the temperature and time of calcination. The optimal conditions for the formation of a porous layer with good mechanical strength was found to be treatment of the coated fiber at 1050 °C for 1 h. Figure 2 shows the scanning electron microscopy (SEM) images of the BCFZ hollow-fiber membrane coated by BCFZ-Pd. It can be seen from Figure 2a and b that BCFZ-Pd layer, with the thickness of about 40 μm, is tightly attached to the outer surface of the BCFZ hollow-fiber membrane. And no development of cracks was observed on the dense part of the BCFZ membrane after the coating process. Moreover, the outer BCFZ-Pd layer sintered at 1050 °C for 1 h is still porous. Therefore, a larger surface area is obtained and a higher catalytic activity can be expected. Figure 2c demonstrates the surface morphology of BCFZ hollow-fiber membrane coated by BCFZ-Pd surface layer. It can be seen that the outer side of the hollow fiber is well coated by surface layer (BCFZ-Pd) along the whole length, although some cracks are observed due to shrinking of the coating by the heat treatment. The magnified image (Figure 2d) shows that the BCFZ-Pd particles are connected with each other forming a three-dimensional network, which ensures the necessary mechanical strength and porosity.

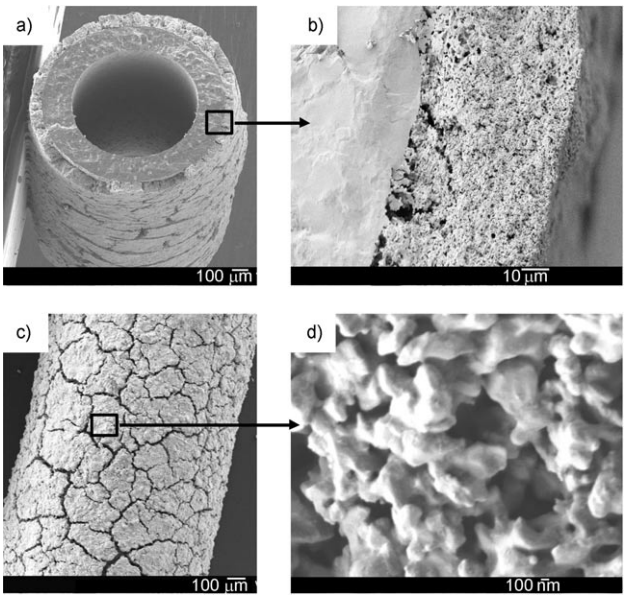

Figure 2. SEM micrographs of the BCFZ hollow-fiber membrane with a BCFZ-Pd layer treated at 1050 °C for 1 h. (a, b) cross-section, and (c, d) outer surface of the modified hollow-fiber membrane before use in the membrane reactor.

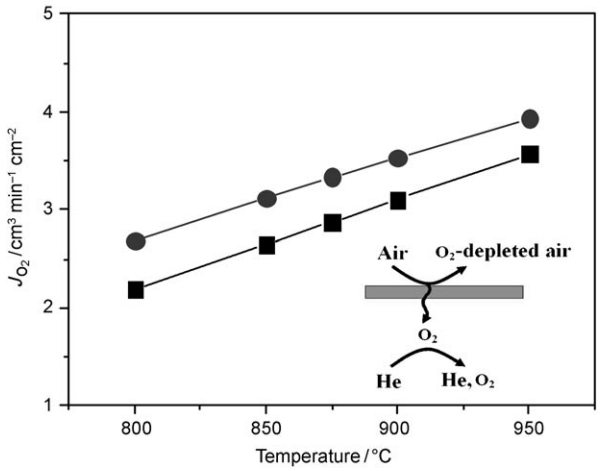

Figure 3. Oxygen permeation fluxes (J_{O_2}) of a BCFZ hollow-fiber membrane with (●) or without (■) a BCFZ-Pd porous layer as a function of temperature using He as the sweep gas. Core side: $F_{air} = 150\ cm^3\ min^{-1}$. Shell side: $F_{He} = 49\ cm^3\ min^{-1}$ and $F_{Ne} = 1.0\ cm^3\ min^{-1}$. Membrane area: 0.86 cm^2.

It is very important to make sure that the hollow-fiber membrane is still gastight along its whole length after the catalyst coating process. Therefore, after the fiber was installed in the high-temperature reactor, a large pressure gradient across the membrane was established by increasing the pressure on the core side. It was found that, at room temperature, there is not any increase in pressure on the shell side when the pressure on the core side was increased from 1 to 5 bar, indicating the membrane is still gastight after the coating process. During the measurements, air was fed to the core side. At high temperature, oxygen can be selectively transported from the core side to the shell side, but nitrogen cannot if the membrane is gastight. So nitrogen from air can work as the impermeable gas to indicate whether the membrane is gastight or not. There is no obvious nitrogen detected by gas chromatography from the shell side for all hollow-fiber membranes we have investigated, which indicates they are all gastight.

Figure 3 demonstrates the temperature dependence of the oxygen permeation flux J_{O_2} of the blank and surface-modified BCFZ membranes, using He as the sweep gas. It can be seen that J_{O_2} increases with increasing temperature for both membranes. However, J_{O_2} of the coated membrane is only by about 10% higher than that of the uncoated one. According to our previous studies,[13] the permeation flux through the BCFZ hollow-fiber membrane is controlled by both the bulk diffusion of oxygen ions and the surface exchange processes. The BCFZ-Pd porous layer on the permeation side can provide more sites for the association of oxygen ions to molecular oxygen followed by desorption, leading to a higher surface exchange rate. So a slight increase of the oxygen permeation flux is observed due to surface enlargement by the BCFZ-Pd porous layer onto BCFZ membrane surface.

One promising application of the perovskite membranes is their use as a reactor for the partial oxidation of hydrocarbons.[4,5] In this case, another kind of surface reaction between the permeated oxygen species and hydrocarbon is involved. So it is interesting to investigate the effect of surface modification of the perovskite membrane on the oxygen permeation rate by using a reactive gas such as CH_4 as sweep gas. Figure 4 presents J_{O_2} at different temperatures of the blank and coated BCFZ hollow-fiber membranes when feeding dilute methane on the permeation side. In comparison with the blank BCFZ membrane, J_{O_2} increased dramati-

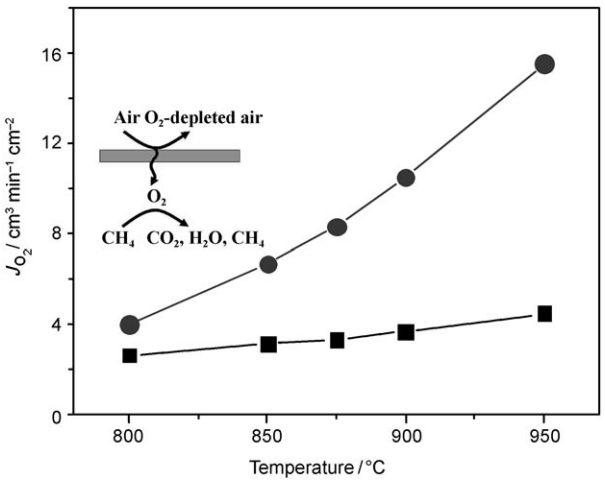

Figure 4. Oxygen permeation fluxes (J_{O_2}) of a BCFZ hollow-fiber membrane with (●) or without (■) a BCFZ-Pd porous layer as a function of temperature with dilute methane on the permeation side for oxygen consumption. Core side: $F_{air} = 150\ cm^3\ min^{-1}$. Shell side: $F_{He} = 39\ cm^3\ min^{-1}$, $F_{CH_4} = 10\ cm^3\ min^{-1}$, and $F_{Ne} = 1.0\ cm^3\ min^{-1}$. Membrane area: 0.86 cm^2.

cally from 4.5 to 15.5 mL min^{-1} cm^{-2} at 950 °C after coating with a porous BCFZ-Pd layer. This experimental finding can be understood as follows: When feeding diluted methane to the permeation side, the main surface reaction is methane oxidation ($CH_4+4O^{2-}\rightarrow CO_2+2H_2O+8e^-$). In the case of coating by the catalytically active BCFZ-Pd porous layer with a large surface area, the permeated oxygen species can be consumed faster due to the higher catalytic activity of surface layer for methane oxidation; therefore, a lower oxygen partial pressure can be obtained, which could be measured by gas chromatography, as shown in Figure 5. It can be seen from Figure 5 that the oxygen partial pressure above the coated membrane on the methane side is clearly lower than that of the blank BCFZ membrane. This experimental finding shows that the Pd-containing BCFZ coating effectively catalyses the combustion of methane. Thus, a larger oxygen partial pressure gradient was established across the coated membrane and the oxygen permeation rate is enhanced based on the Wagner equation.[1]

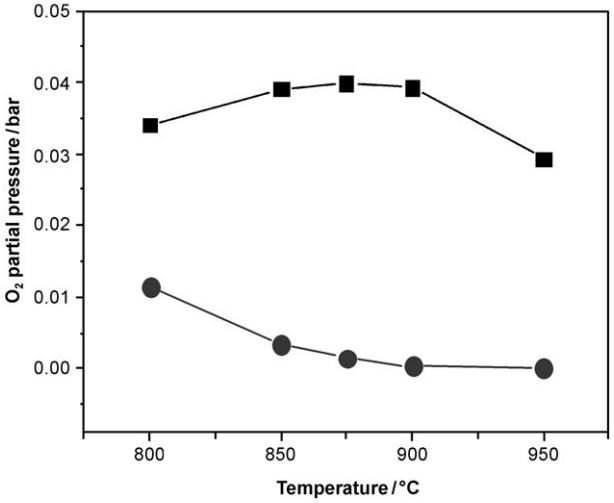

Figure 5. Temperature dependence of the residual oxygen partial pressure on the permeation side of BCFZ membrane with (●) or without (■) a BCFZ-Pd porous coating measured by gas chromatography (see the experimental conditions given in Figure 4).

Methane combustion over cobalt-containing perovskite, which is one of the most reducible perovskites, has been extensively investigated in recent years.[11,12] The partial reduction of Co^{3+} to Co^{2+} in perovskite leads to large amounts of active sites (oxygen vacancies) for oxygen adsorption and, thus, a high catalytic activity towards methane oxidation.[14] When comparing the fresh (Figure 2d) and spent (Figure 6a) one can see that the spent coating contains spherical particles of about 100–200 nm. From the light appearance of the spherical particles, due to a higher emission of secondary electrons, it can be concluded that they are enriched with heavy metals. Correspondingly, EDXS of the spent coating in STEM mode shows an inhomogeneous distribution of Pd

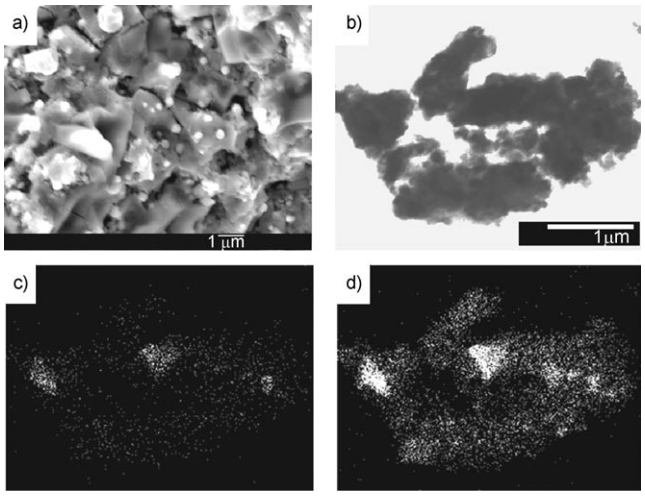

Figure 6. Spent BCFZ-Pd coating after studying the oxygen permeation at 950 °C (see Figure 4): a) Secondary electron micrograph, b) STEM bright-field micrograph, and the corresponding elemental distribution images of palladium (c) and cobalt (d).

and Co (Figure 6b–d). Different from the fresh particles before measurement, in which all the related elements were homogeneously distributed (see Figure S1c to h, Supporting Information), the Co-enriched phase and Co–Pd co-enriched phase were identified (Figure 6c and d). The presence of the Co–Pd co-enriched phase implies an interaction between Co and Pd. It is reported that the presence of Pd increased the reducibility of cobalt ions in a Pd–Co/Al_2O_3 catalyst.[12] Here, the addition of Pd into a Co-containing perovskite lattice enhances reducibility of the cobalt ions and, thus, leads to a higher catalytic activity towards methane oxidation.

From the above results, it can be seen that the BCFZ hollow-fiber membrane with BCFZ-Pd catalytic porous layer exhibits higher oxygen permeability, so a better performance can be expected when it is used as a membrane reactor. Herein, we have evaluated the catalytically modified BCFZ hollow-fiber membrane for hydrogen production by water splitting in a membrane reactor: on one side of the membrane water is thermally dissociated into hydrogen and oxygen according to $H_2O\rightleftarrows H_2+{}^1/_2\,O_2$. The latter can be removed in situ by the oxygen-permeable membrane and then consumed by methane oxidation on the other side according to $CH_4+2O_2\rightarrow CO_2+2H_2O$. Clearly, the hydrogen production rate after steam condensation in the retentate is related to three processes: water dissociation, oxygen transport through the membrane, and oxygen consumption on the permeation side. Figure 7 shows the temperature dependence of hydrogen production rates for the blank and surface-modified BCFZ membrane reactors. It was found that the hydrogen production rate increases as the temperature rises from 800 to 950 °C for both membranes. With increasing temperature, the equilibrium constant of the endothermic water splitting will increase, and the oxygen removal rate from the water dissociation system will also increase due to the increased oxygen permeability of the membrane. There-

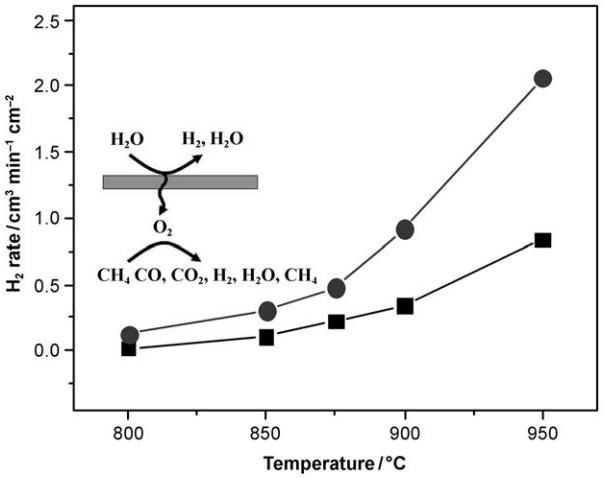

Figure 7. H_2 production rates as a function of temperature on a BCFZ hollow-fiber membrane with (●) or without (■) a BCFZ-Pd porous layer. Core side: $F_{H_2O}=30\ cm^3 min^{-1}$ and $F_{He}=10\ cm^3 min^{-1}$. Shell side: $F_{He}=39\ cm^3 min^{-1}$, $F_{CH_4}=10\ cm^3 min^{-1}$, and $F_{Ne}=1.0\ cm^3 min^{-1}$. Membrane area: 0.86 cm^2.

fore, the hydrogen production rate becomes higher with increasing temperature. As discussed above, compared with the blank BCFZ membrane, the surface-modified BCFZ hollow-fiber membrane shows higher catalytic activity towards methane oxidation, leading to higher oxygen permeation rate. Thus, a higher hydrogen production rate was obtained after the surface of BCFZ membrane was modified by a BCFZ-Pd catalytic porous layer. It can be seen from Figure 7 that the hydrogen production rate has been improved from 0.7 to 2.1 $mL min^{-1} cm^{-2}$ at 950 °C after depositing a BCFZ-Pd porous layer onto the BCFZ membrane.

Conclusion

A BCFZ hollow-fiber membrane that is surface modified by a catalytically active BCFZ-Pd porous layer shows a high catalytic activity in hydrocarbon combustion. The oxygen permeation flux of the surface-modified BCFZ membrane was increased by 3.5 times compared with that of the blank BCFZ membrane when adding oxygen-consuming CH_4 instead of an inert sweep gas such as He to the permeation side. When the surface-modified BCFZ membrane was used as a reactor to shift the equilibrium of water dissociation for hydrogen production, a higher H_2 production rate was obtained due to its higher oxygen permeability. We have demonstrated that by modifying the oxygen-permeable, hollow-fiber BCFZ perovskite membrane with a proper catalytic porous layer not only the oxygen permeation flux can be enhanced, but also a better reactor performance can be obtained.

Experimental Section

BCFZ-Pd perovskite powder was prepared by a combined citric acid and ethylenediaminetetraacetic acid (EDTA) complexing method.[15] The calculated amounts of $Ba(NO_3)_2$, $Pd(NO_3)_2$, and $ZrO(NO_3)_2$ powder were dissolved in an aqueous solution of $Co(NO_3)_2$ and $Fe(NO_3)_3$ followed by the addition of EDTA and citric acid with the molar ratio of EDTA/citric acid/metal cations = 1:1.5:1. After agitation for a certain time, the pH value of the solution was adjusted to around nine by adding NH_4OH. The solution was then heated in the temperature range of 120–150 °C under constant stirring to obtain a gel. Further heat treatment was applied at 950 °C for 10 h to obtain BCFZ-Pd perovskite powder with the final composition.

The crystal structure of BCFZ-Pd perovskite powder was investigated by using a Philips X′pert-MPD instrument with $Cu_{K\alpha}$ radiation. TEM was performed on a JEOL JEM-2100F field-emission instrument. An Oxford Instruments INCA-200-TEM system with an ultra-thin window was attached to the microscope to allow for elemental analysis using EDXS. The surface morphology of BCFZ hollow-fiber membrane coated with a BCFZ-Pd layer was characterized by using a JEOL JSM-6700F field-emission scanning electron microscope.

The dense BCFZ hollow-fiber membranes were manufactured by phase-inversion spinning followed by sintering.[13] The sintered fiber had a wall thickness of around 0.17 mm with an outer diameter of 1.10 mm and an inner diameter of 0.76 mm. The BCFZ-Pd slurry was prepared by mixing BCFZ-Pd powder with water in a mortar followed by milling. The BCFZ-Pd porous layer can be obtained by brushing the above slurry onto the outer surface of the central 3 cm of BCFZ membrane followed by heating at 1050 °C for 1 h. To obtain the isothermal condition, two ends of the fiber were coated with Au paste followed by sintering at 950 °C and thus a dense Au film that is not permeable to oxygen was obtained.

The oxygen permeation experiments were carried out in a high-temperature permeator as described in our previous work.[16] Synthetic air or steam diluted by He was fed into the core side and a mixture of CH_4, Ne, and He was fed into the shell side. All gas flows were controlled by mass flow controllers (Bronkhorst), which were calibrated by using a soap bubble meter before measurements. The total flow rate of the effluents on shell side was calculated by using Ne as an internal standard. The concentrations of the gases at the exit of the reactor were determined by an on-line gas chromatograph (Agilent 6890). The oxygen permeation rate can be obtained based on the change of oxygen concentration on air side between the inlet and outlet. H_2 production rate on the core side was calculated from the total flow rate F_{core} ($mL min^{-1}$), hydrogen concentration $c(H_2)$, and membrane area S (cm^2) by using Equation (1):

$$J(H_2) = \frac{F\mathrm{core} \times c(H_2)}{S} \quad (1)$$

Acknowledgements

The authors gratefully acknowledge the financial support of the BMBF for the project 03C0343A SynMem under the auspices of ConNeCat.

[1] a) W. S. Yang, H. H. Wang, X. F. Zhu, L. W. Lin, *Top. Catal.* **2005**, *35*, 155–167; b) J. Sunarso, S. Baumann, J. M. Serra, W. A. Meulenberg, S. Liu, Y. S. Lin, J. C. Diniz da Costa, *J. Membr. Sci.* **2008**, *320*, 13–41; c) Y. T. Liu, X. Y. Tan, K. Li, *Catal. Rev. Sci. Eng.* **2006**, *48*, 145–198; d) C. S. Chen, S. J. Feng, S. Ran, D. C. Zhu, W. Liu, H. J. M. Bouwmeester, *Angew. Chem.* **2003**, *115*, 5354–5356; *Angew. Chem. Int. Ed.* **2003**, *42*, 5196–5198; e) R. Merkle, J. Maier, *Angew. Chem.* **2008**, *120*, 3936–3958; *Angew. Chem. Int. Ed.* **2008**, *47*, 3874–3894.

[2] a) J. Caro, K. J. Caspary, C. Hamel, B. Hoting, P. Kölsch, B. Langanke, K. Nassauer, T. Schiestel, A. Schmidt, R. Schomäcker, A.

Seidel-Morgenstern, E. Tsotsas, I. Voigt, H. H. Wang, R. Warsitz, S. Werth, A. Wolf, *Ind. Eng. Chem. Res.* **2007**, *46*, 2286–2294; b) H. H. Wang, C. Tablet, A. Feldhoff, J. Caro, *Adv. Mater.* **2005**, *17*, 1785–1788; c) J. Martynczuk, M. Arnold, H. H. Wang, J. Caro, A. Feldhoff, *Adv. Mater.* **2007**, *19*, 2134–2140.

[3] P. N. Dyer, R. E. Richards, S. L. Russek, D. M. Taylor, *Solid State Ionics* **2000**, *134*, 21–33.

[4] a) H. J. M. Bouwmeester, *Catal. Today* **2003**, *82*, 141–150; b) J. T. Ritchie, J. T. Richardson, D. Luss, *AIChE J.* **2001**, *47*, 2092–2101.

[5] a) F. T. Akin, Y. S. Lin, *J. Membr. Sci.* **2002**, *209*, 457–467; b) H. H. Wang, Y. Cong, W. S. Yang, *Catal. Lett.* **2002**, *84*, 101–106.

[6] J. P. Perez-Ramirez, B. Vigeland, *Angew. Chem.* **2005**, *117*, 1136–1139; *Angew. Chem. Int. Ed.* **2005**, *44*, 1112–1115.

[7] a) J. F. Vente, W. G. Haije, Z. S. Rak, *J. Membr. Sci.* **2006**, *276*, 178–184; b) H. Kusaba, Y. Shibata, K. Sasaki, Y. Teraoka, *Solid State Ionics* **2006**, *177*, 2249–2253; c) V. V. Kharton, A. Kovalevsky, A. A. Yaremchenko, F. M. Figueiredo, E. N. Naumovich, A. L. Shaulo, F. M. B. Marques, *J. Membr. Sci.* **2002**, *195*, 277–287; d) S. Lee, K. S. Lee, S. K. Woo, J. W. Kim, T. Ishihara, D. K. Kim, *Solid State Ionics* **2003**, *158*, 287–296; e) A. Thursfield, I. S. Metcalfe, *J. Membr. Sci.* **2007**, *288*, 175–187.

[8] K. Gerdes, D. Luss, *AIChE J.* **2007**, *53*, 1389–1391.

[9] a) H. Q. Jiang, H. H. Wang, F. Y. Liang, S. Werth, T. Schiestel, J. Caro, *Angew. Chem.* **2009**, *121*, 3027–3030; *Angew. Chem. Int. Ed.* **2009**, *48*, 2983–2986; b) H. Q. Jiang, H. H. Wang, S. Werth, T. Schiestel, J. Caro, *Angew. Chem.* **2008**, *120*, 9481–9484; *Angew. Chem. Int. Ed.* **2008**, *47*, 9341–9344; c) H. H. Wang, C. Tablet, T. Schiestel, S. Werth, J. Caro, *Catal. Commun.* **2006**, *7*, 907–912; d) H. H. Wang, S. Werth, T. Schiestel, J. Caro, *Angew. Chem.* **2005**, *117*, 7066–7069; *Angew. Chem. Int. Ed.* **2005**, *44*, 6906–6909; e) H. H. Wang, T. Schiestel, C. Tablet, M. Schroeder, J. Caro, *Solid State Ionics* **2006**, *177*, 2255–2259.

[10] a) S. D. Peter, E. Garbowski, V. Perrichon, M. Primet, *Catal. Lett.* **2000**, *70*, 27–33; b) H. H. Wang, A. Feldhoff, J. Caro, T. Schiestel, S. Werth, *AIChE J.* **2009**, *55*, 2657–2664.

[11] a) O. Demoulin, M. Navez, P. Ruiz, *Catal. Lett.* **2005**, *103*, 149–153; b) K. Persson, A. Ersson, K. Jansson, J. L. G. Fierro, S. G. Jaras, *J. Catal.* **2006**, *243*, 14–24; c) B. Bialobok, J. Trawczynski, W. Mista, M. Zawadzki, *Appl. Catal. B-Environmental* **2007**, *72*, 395–403.

[12] A. Sarkany, Z. Zsoldos, G. Stefler, J. W. Highttower, L. Guczi, *J. Catal.* **1995**, *157*, 179–189.

[13] T. Schiestel, M. Kilgus, S. Peter, K. J. Caspary, H. H. Wang, J. Caro, *J. Membr. Sci.* **2005**, *258*, 1–4.

[14] M. Arnold, Q. Xu, F. D. Tichelaar, A. Feldhoff, *Chem. Mater.* **2009**, *21*, 635–640.

[15] a) Z. P. Shao, W. S. Yang, Y. Cong, H. Dong, J. H. Tong, G. X. Xiong, *J. Membr. Sci.* **2000**, *172*, 177–188; b) L. Yang, Z. T. Wu, W. Q. Jin, N. P. Xu, *Ind. Eng. Chem. Res.* **2004**, *43*, 2747–2752.

[16] H. H. Wang, P. Kölsch, T. Schiestel, C. Tablet, S. Werth, J. Caro, *J. Membr. Sci.* **2006**, *284*, 5–8.

Received: September 9, 2009
Revised: February 2, 2010
Published online: May 21, 2010

